JOURNAL OF MATERIALS SCIENCE **35** (2000) 3479 – 3495

Copper deposition during the corrosion of aluminum alloy 2024 in sodium chloride solutions

H. M. OBISPO, L. E. MURR, R. M. ARROWOOD, E. A. TRILLO
Department of Metallurgical and Materials Engineering, and FAST Center, The University of Texas at El Paso, El Paso, Texas 79968-0520 USA

Copper and copper-rich particle clusters were observed to deposit on aging aircraft skin material (Al 2024 sheet coupons) after corrosion immersion experiments for 5 days in acidic (pH 3) neutral (pH ∼ 6), and basic (pH 11) 0.6 M NaCl solutions. SEM analysis employing an EDX spectrometer showed a propensity of large Cu particle clusters on Fe-rich or Fe-containing areas while a TEM inventory of second-phase particles in the alloy sheet showed a propensity of Al-Fe-Cu-Mn and Al-Cu-Si particles along with Al-Cu-Mg and Al-Cu-Fe-Mn-Si particles and particle clusters. A modified replication technique was used to lift particles from the corroded coupon surfaces. TEM analysis employing an EDX spectrometer showed a wide range of copper deposits exhibiting microdendritic morphologies in basic and neutral environments, and botryoidal (or nodular) morphologies in acidic environments. The plating or cementation of copper from solution as an electrochemical displacement reaction appears to be a major contributor to the pitting corrosion of 2024 aluminum alloy. © *2000 Kluwer Academic Publishers*

1. Introduction

The corrosion of dilute aluminum alloys containing copper, especially aircraft alloys such as 2024 aluminum (∼4 weight percent Cu), especially on older (or aging) military and commercial aircraft, has been an area of particular interest in recent years [1]. Key issues involved in copper-containing alloys appear to involve galvanic couples set up between copper-rich, intermetallic inclusions/precipitates and the adjacent copper-depleted matrix [2–5]. In recent work by Buchheit, *et al.* [5], S-phase (Al_2CuMg) particles (0.5 to 0.7 μm in size) exhibited severe dealloying which resulted in the formation of Cu-rich remnants. Some particle remnants remained intact and induced pitting at their periphery. This copper redistribution was also recently studied by Dimitrov, *et al.* [6] on an aluminum alloy 2024 sample in 0.6 M NaCl solutions.

The implications of these investigations [2–6] have been that nanoporous copper-rich remnants which are formed by dealloying at copper-rich inclusions are redistributed on the aluminum surface, but are not intimately attached. In addition, copper-rich remnant particles have been observed in the scanning electron microscope on aluminum alloy surfaces [5] to range in size from 0.01 to 0.1 μm.

In recent particle-induced corrosion studies by Wei, *et al.* [7, 8], not only did Al_2CuMg particles react and exhibit the characteristic dealloyed microstructures [5, 6], but the surrounding matrix was observed to dissolve and release Cu^{2+} ions into the NaCl solution. Al-Cu-Mn-Fe particles were also observed to act as cathodic sites relative to the matrix; leading to the reduction of Cu^{2+} ions dissolved in the NaCl solution. Copper plating was observed on the Al-Cu-Mn-Fe particles in contrast to the Al-Cu-Mg-containing particles which acted as anodic sites, losing Al and Mg through dissolution in the early stage of corrosion; becoming more cathodic as Cu was left behind.

In summarizing the more recent studies of pitting corrosion in aluminum alloy 2024 [5–8], it would appear that some inclusions behave anodically or cathodically and undergo selective corrosion reactions in NaCl solutions which variously produce Cu^{2+} ions in solution, elemental Cu debris particles which are sometimes redistributed over the aluminum alloy surface, and the plating or growth of Cu nodules on specific (cathodic) inclusions such as Al-Cu-Mn-Fe-containing particles. In addition, pitting induced by inclusions was found to be pH dependent [7].

In this investigation we utilized a replica-based lift-off technique to extract spatially intact copper particles from aluminum alloy 2024 surfaces after exposure to NaCl solutions, ranging in pH from 3 to 11, and to examine them in detail using transmission and scanning electron microscopy (TEM and SEM). Associated particle chemistries were also examined in the TEM using energy-dispersive X-ray spectrometry and selected-area electron diffraction.

2. Experimental details

Aluminum alloy 2024 aircraft body skin (sheet) samples were obtained from aging KC-135 aircraft and sectioned into test coupons measuring 1.9 cm on a side. These coupons were polished to a uniform surface finish with SiC paper and fine polished with colloidal

SiO_2 (0.02 μm). Representative coupons were then immersed in 3.5% (0.6 M) NaCl solutions for 120 h (5 days). Three solution categories (using deionized water) were developed as comparative test environments: 1) an original (neutral) 0.6 M NaCl solution with a pH of ~6, 2) an acidic 0.6 M NaCl solution containing HCl to adjust the pH to 3, 3) a basic 0.6 M NaCl solution containing NaOH to adjust the pH to 11. The tests were conducted at a uniform temperature of ~22°C. After immersion in these three solutions (which were not stirred), the test coupons were rinsed in distilled water and ethanol. The solutions were not stirred in order to keep any remnant copper particles from significantly redistributing.

Potentiostatic tests were also performed on the neutral NaCl solution coupons at −200 mV (the highest current value in the anodic region of the curve) versus SCE; for a period of 3 minutes at 22°C.

Test coupons were initially examined by scanning electron microscopy (SEM). Several different scanning electron microscopes were employed in this investigation. The SEMs were also fitted with energy-dispersive X-ray analysis systems so that copper and copper-rich features could be identified along with other features. However in some cases particle clusters/reaction products were difficult to view at higher magnifications because of charging effects which could only be eliminated by metal (gold) sputtering of the surface.

In order to enhance the particle and surface debris resolution, a replica-based lift-off technique was employed as described previously for examining debris particles on space craft surfaces [9, 10]. In this technique, illustrated schematically in Fig. 1, an acetate-based plastic replicating tape is moistened on one side with acetone and pressed lightly against the coupon surface, allowed to dry, and then stripped off (using an acetone soluable, sticky tape); removing any adhering, attached or detached particulates, products, or debris which adhere to

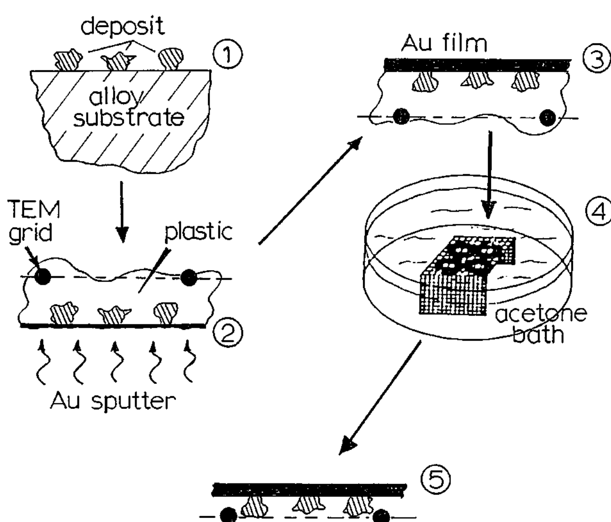

Figure 1 Schematic representation of replication-based, lift-off process for viewing surface particles (1) in the TEM. The plastic strips the surface features (2) which are stabilized in a thin, sputtered gold support film (3). The plastic matrix is washed in an acetone bath (4) allowing the TEM grid (3 mm diameter 100 or 200 mesh Cu or Ni screen) to settle onto the gold support holding the surface particles/features (5). (After Miglionico, *et al.* [9].)

the replica tape. A thin (~0.02 μm thick) gold film was sputtered onto the stripped surface (Fig. 1) and 3 mm copper or nickel screen-mesh grids (for transmission electron microscope (TEM) film support) were placed on the acetate plastic surface, turned up-side down and placed on a Ni/Cu alloy wire screen support in a petri dish containing acetone. This petri dish was allowed to sit overnight to wash away the acetate plastic, leaving the spatially imbedded particulates, etc. adhering to the gold support film on the 3 mm TEM screen (mesh) grids. The 3 mm screen mesh grids were then examined in a Hitachi H-8000 analytical TEM fitted with an energy-dispersive X-ray (EDX) spectrometer, at an accelerating voltage of 200 kV. The nickel screen grids were employed as a precaution to assure that the copper grids were not contributing false peaks to the EDX spectrum, and the sputter-coated gold substrate supporting the spatially intact surface products acted as an internal calibration in addition to providing adequate conductivity to avoid particle charging in the fine-focused electron beam at high magnifications.

To further identify surface features and to confirm the stripping of surface products/particles, the TEM grid samples were also examined in the SEM. In addition, surfaces on the test coupons which were examined in the SEM prior to application of the replica/stripping process (Fig. 1), were re-examined after stripping, so that the entire process sequence could be observed in detail, and observations in the TEM correlated with SEM observations.

Test coupons were also ground to thicknesses of roughly 0.2 mm and 3 mm disks punched for preparing TEM samples. These punched disks were electropolished to electron transparency in a Tenupole-3 dual jet electropolisher employing a solution of 20% nitric acid in methanol; at −30°C. These TEM specimens of the original aluminum alloy 2024 test coupons were extensively examined to develop a reasonably complete inventory of second-phase particles which were qualitatively identified using EDX spectra and selected-area electron diffraction (SAED). The qualitative precipitate analyses involving EDX spectra in the TEM were then used to evaluate the EDX spectra obtained in the SEM for reaction products and other features observed for specimens immersed in the test solutions.

3. Results and discussion

3.1. TEM inventory of second-phase particles

Buchheit, *et al.* [5] observed that in their 2024-T3 aluminum alloy there were four primary types of second-phase particles; with the Al_2 Cu Mg-type the most predominant. Urishiho and Sujimoto [7] and Garner and Tromans [3] among others have described how Cu concentration in second-phase particles and the depletion of Cu in certain microstructural regions develops galvanic cells which initiate localized attack. As a consequence of these issues, we thought it prudent to develop an inventory of second-phase particles in the experimental 2024 aluminum alloy since it came from an older aircraft where the composition and temper were probably different from others.

Five prominent regimes of large (>0.5 μm diameter) second-phase particles or particle clusters were observed by TEM: Al-Cu-Fe-Mn, Al-Cu-Si, Al-Cu-Mg, Al-Cu-Fe-Mn-Si, and Al-Cu-Fe. The first two regimes represented roughly 65% of the particle inventory while the Al-Cu-Mg particles represented roughly 18%. The Al-Cu-Fe-Mn-Si particles represented around 8% while the remaining 9% consisted of Al-Cu-Fe along with Al-Cu-Fe-Si and Al-Cu-Mn particles. Figs 2–4 show some typical examples for a few of these regimes of particles or particle-clusters. In Fig. 2, the Al-Cu-Fe-Mn-Si regime is different from the particles in the cluster of Fig. 3b and c, although Fig. 2b and Fig. 3c are similar, but very different from Fig. 3b where Al and Si are very prominent and Cu is suppressed. Particle d in Fig. 3 contains no Si. These particles are similar to those recently identified in a Rheocast 2024 aluminum alloy and a 2024-T3 aluminum alloy: (Fe, Mn, Cu) Al_x

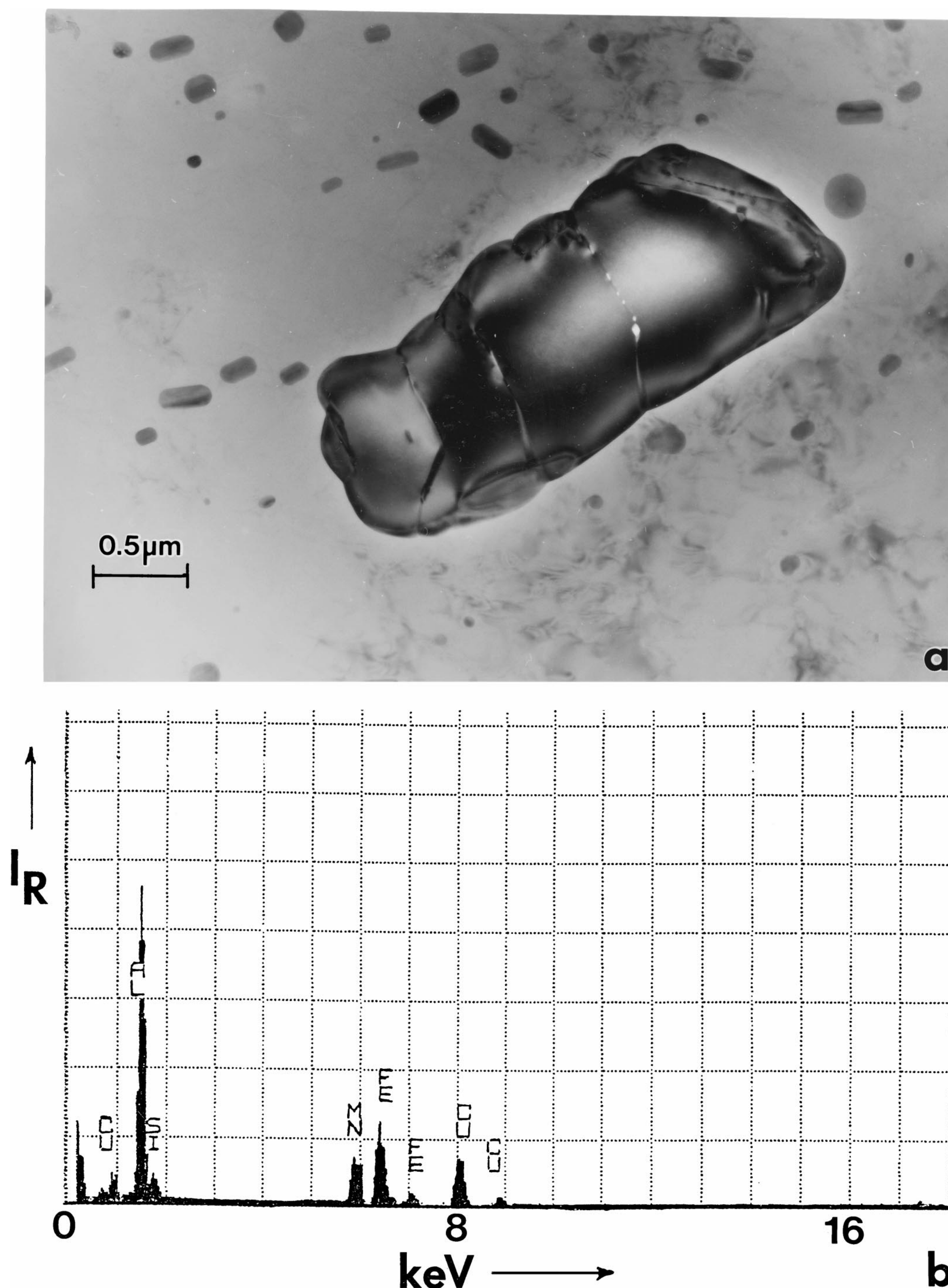

Figure 2 Example of Al-Cu-Mn-Fe-Si second-phase particle in aluminum alloy 2024 from aging aircraft body. (a) Bright-field TEM image. (b) EDX spectrum for particle in (a).

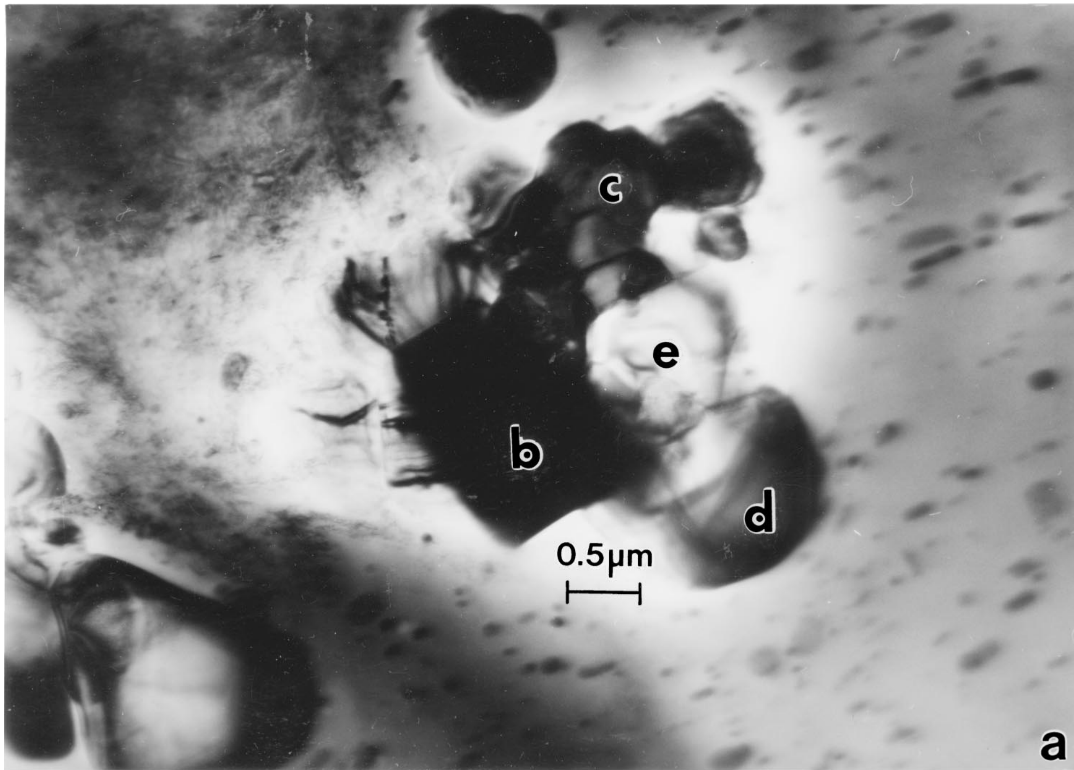

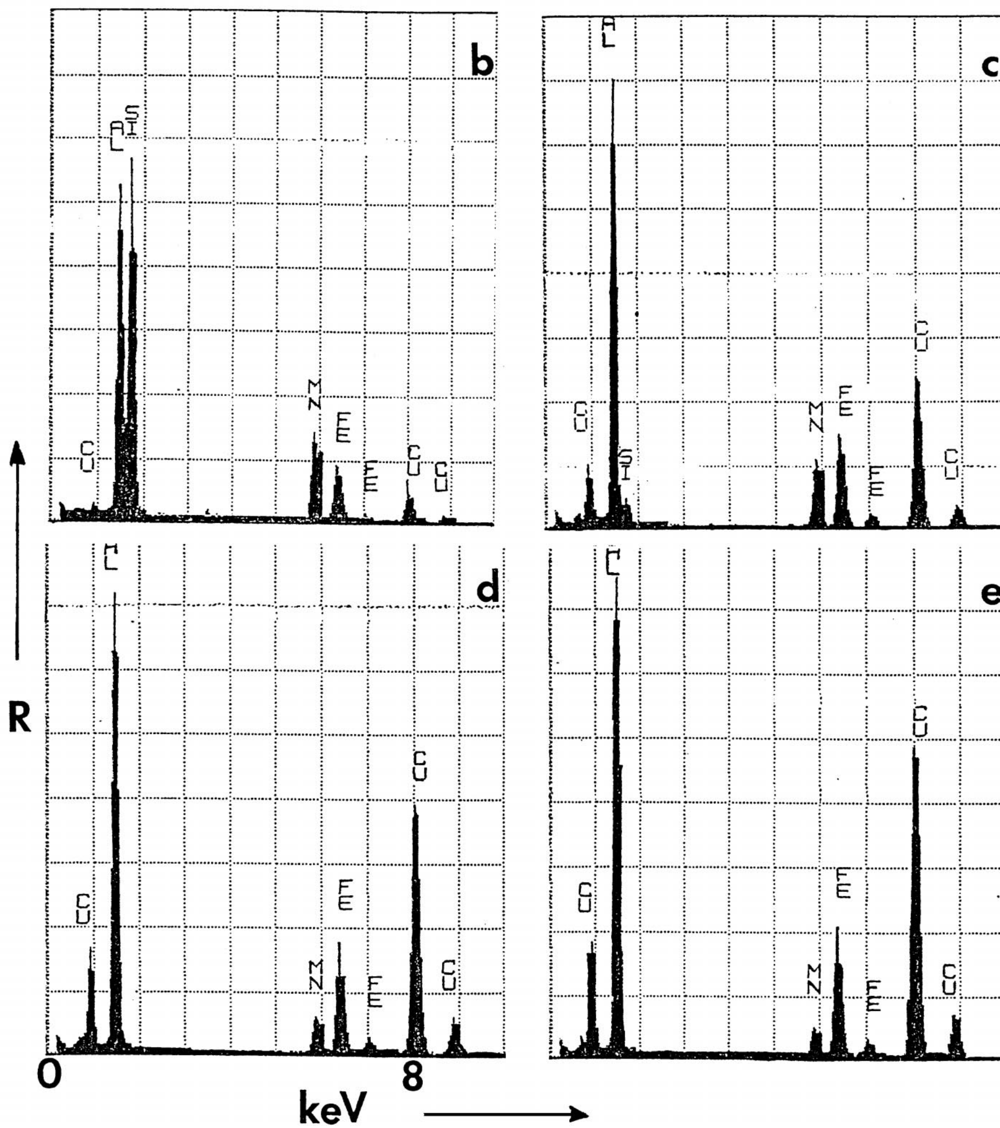

Figure 3 Example of second-phase particle clusters in aluminum alloy 2024. (a) TEM bright-field image of particle cluster. (b) to (e) show EDX spectra corresponding to particles noted in (a) with notations (b) to (e).

[11] and (Fe, Mn)$_x$ Si(Al, Cu)$_y$ [12]. In the latter study [12], the compositions of the Al-Fe-Cu-Mn-Si particles varied considerably from particle to particle and within particle clusters; as shown in Figs 2 and 3. These particles (in Figs 2 and 3) were not as prominent in our alloy; in contrast to the 2024-T3 alloy of Gao, *et al.* [12] and Wei, *et al.* [8].

Fig. 4 shows an example of an Al-Cu-Mg particle which, in contrast to many other studies [5, 6, 8], was not as prominent, especially in contrast to the Al-Cu-Fe-Mn, and Al-Cu-Si particles. While, as noted by Wei, *et al.* [8], particles containing Al, Cu, Fe, and Mn tend to be cathodic, the addition of Si probably changes the activity to anodic with respect to the alloy matrix because Si is more anodic than Mn [13].

3.2. SEM analysis of surface corrosion in neutral, basic, and acidic NaCl solutions

Figs 5 and 6 show some typical surface features and their associated microchemistries for a 2024 aluminum

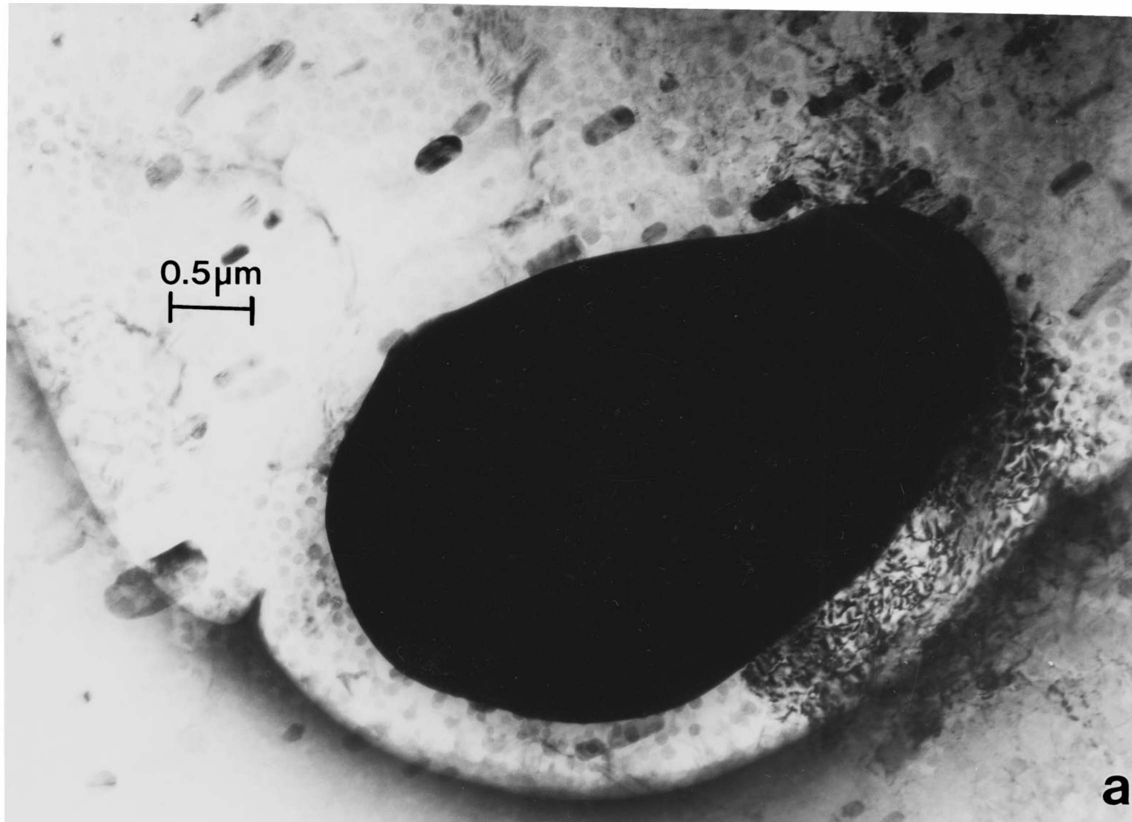

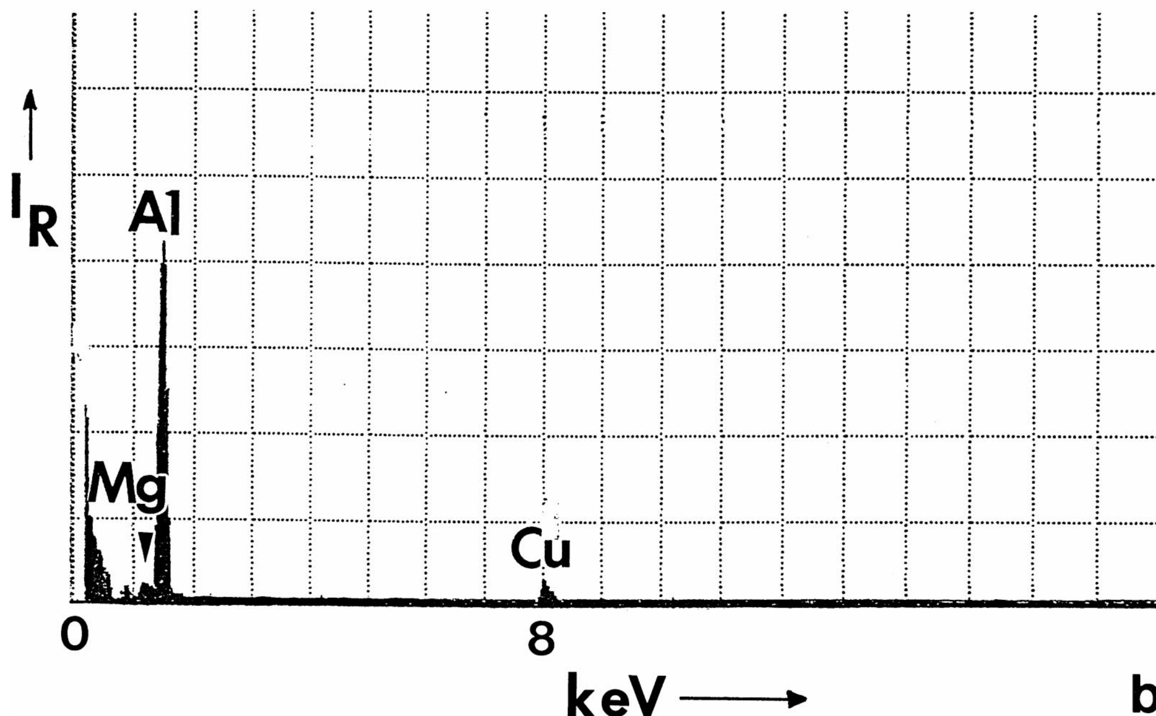

Figure 4 Example of Al-Cu-Mg second-phase particle in aluminum alloy 2024. (a) TEM bright-field image. (b) EDX spectrum of particle in (a).

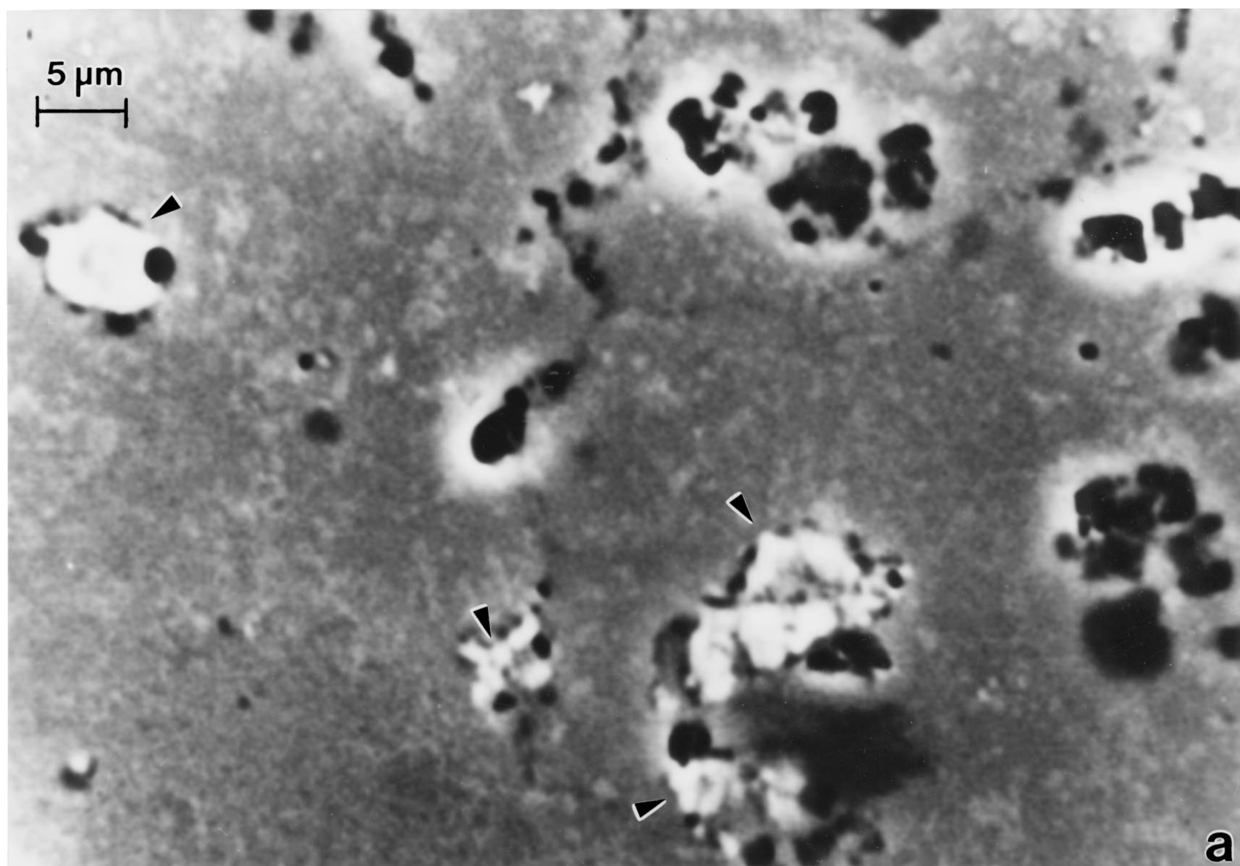

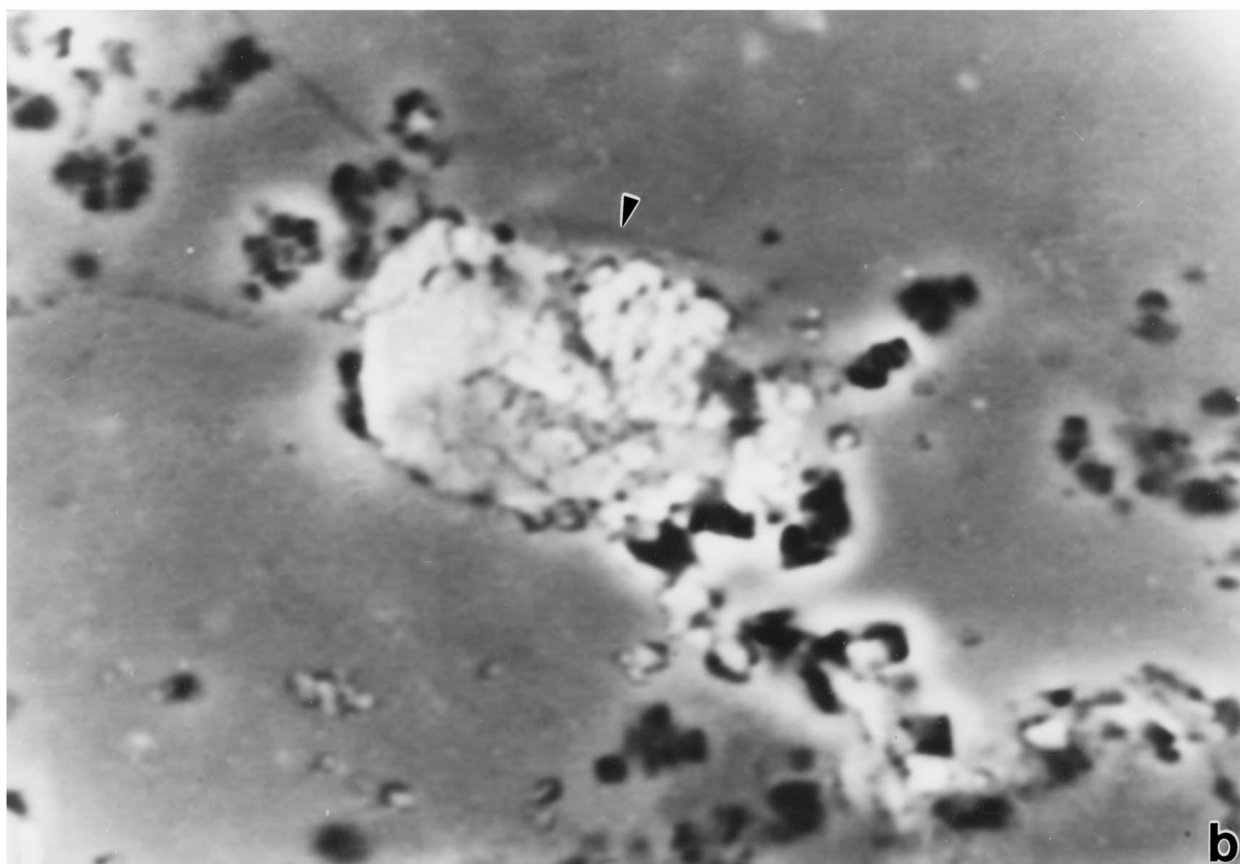

Figure 5 SEM views showing copper/copper-rich particle clusters (arrows) on small particle sites (a) and large particle sites (b) for 2024 aluminum alloy coupon tested (potentiostatically) in neutral NaCl solution for only 3 minutes.

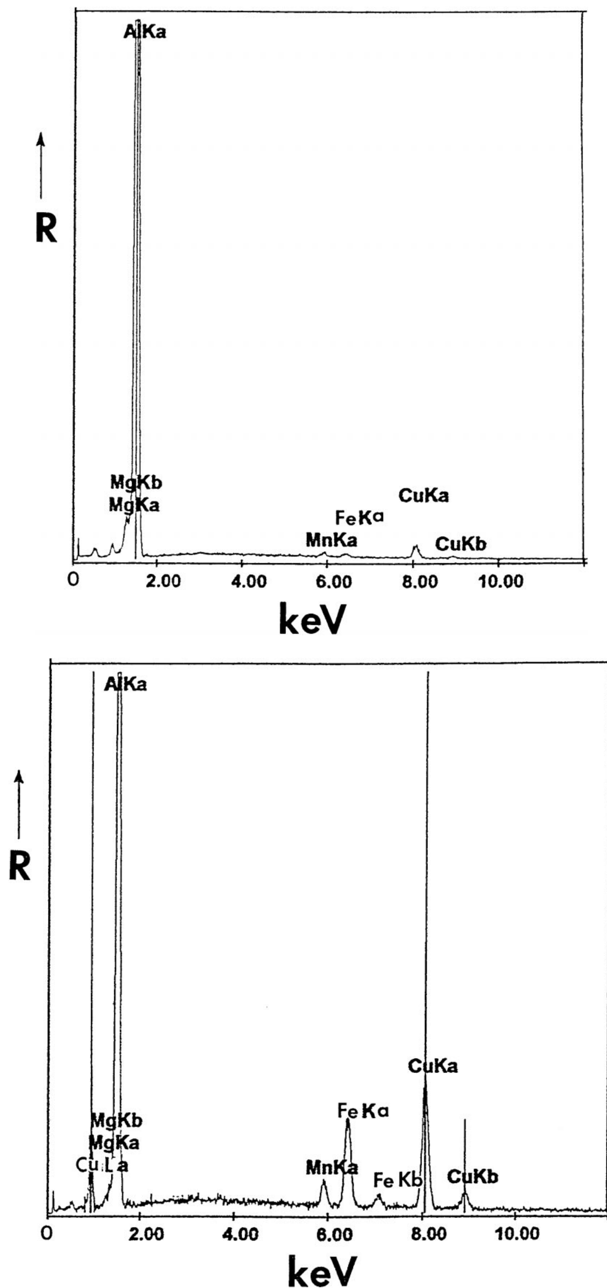

Figure 6 EDX spectra for matrix (a) and the large cluster site (b) corresponding to Fig. 5b.

alloy test coupon in neutral (pH ∼ 6) NaCl solution at a potential of −200 mV for 3 minutes. Many copper-rich clusters were observed to be associated with large corrosion pits or inclusions. Fig. 5b shows a large cluster which exhibits high concentrations of both copper and iron as shown in the corresponding EDX spectra in Fig. 6b. Fig. 6a shows for comparison an EDX spectrum for a region located away from any of the clusters and serves as a reference for the matrix composition.

Fig. 7 shows for comparison similar clusters on a neutral NaCl solution, free corrosion test specimen immersed for 5 days. The cluster indicated by the arrow in Fig. 7a has a microdendritic appearance and was growing in a valley or depression surrounded by what appears to be a corrosion product layer. The corresponding EDX spectrum in Fig. 7b confirms the product layer by the large oxygen peak, which suggests the presence of aluminum oxy-hydroxide ($AlO_x(OH)$) or hydroxide ($AlOH_3$), since hydrogen will not be detected in the EDX spectrum. The cluster area in Fig. 7a is also rich in both iron and copper; similar to Fig. 6b for the corresponding cluster in Fig. 5b.

Fig. 8a shows a very similar cluster of microdendrite-like copper particles in a surface depression on a basic (pH 11) test specimen. The corresponding EDX spectrum in Fig. 8b shows, in comparison with Fig. 7b, significant oxygen characteristic of surface corrosion products, and a very significant copper peak which is associated with the particle cluster. Note that the cluster in Fig. 8a, like those in Figs 7a and 6b, appears to be nucleating and growing at specific surface sites, rather than existing as porous remnants of an emerging second-phase particle. It is interesting to note that iron appears in the site-specific location in each cluster example in Figs 5b and 6b and Figs 7 and 8. Similar observations were also made for acidic NaCl solution test specimens.

3.3. TEM analysis of test coupon surface lift-off replicas

Figs 9 and 10 show examples of the typical appearance of copper clusters apparently growing at a profusion of locations all over the neutral NaCl solution test coupon surfaces. The low and higher-magnification views of the microdendritic features in Fig. 9 are amplified in the higher magnification view of Fig. 10a which, as shown in Fig. 10b, is essentially pure copper. Close inspection of Fig. 9 suggests that these features, stripped from the test coupon surface, are not simply redistributed copper particles from dealloyed, second-phase particles emerging on the coupon surface [5], but rather copper deposition and growth on the surface. These features were confirmed for nearly identical observations made in each NaCl test environment as shown in the basic conditions imaged in Figs 11 and 12, and the acidic example in Fig. 13. In both Figs 12b and 13b the EDX spectra contain nickel and gold peaks (arrows) which are indicative of incidental reflection from the nickel grid supporting the specimens, and the gold film sputtered to imbed the stripped surface features (Fig. 1). Note in Fig. 12a that the selected-area electron diffraction pattern insert shows the deposit to be copper, and composed of a very small grains and larger grain structures; characteristic of a fine, microdendrite structure.

It might also be noted in the EDX spectra shown in Figs 10b, 12b, and 13b that no iron peaks appear in contrast to the EDX spectra for the SEM analysis in Figs 6b, 7b, and 8b. Correspondingly the resolution of much smaller copper clusters in the TEM differs from the larger clusters observed in the SEM, and the SEM observations may be more characteristic of growth on emerging and reacting second-phase particles while the TEM images are more characteristic of copper deposition or cementation; i.e. heterogeneous electrochemical displacement.

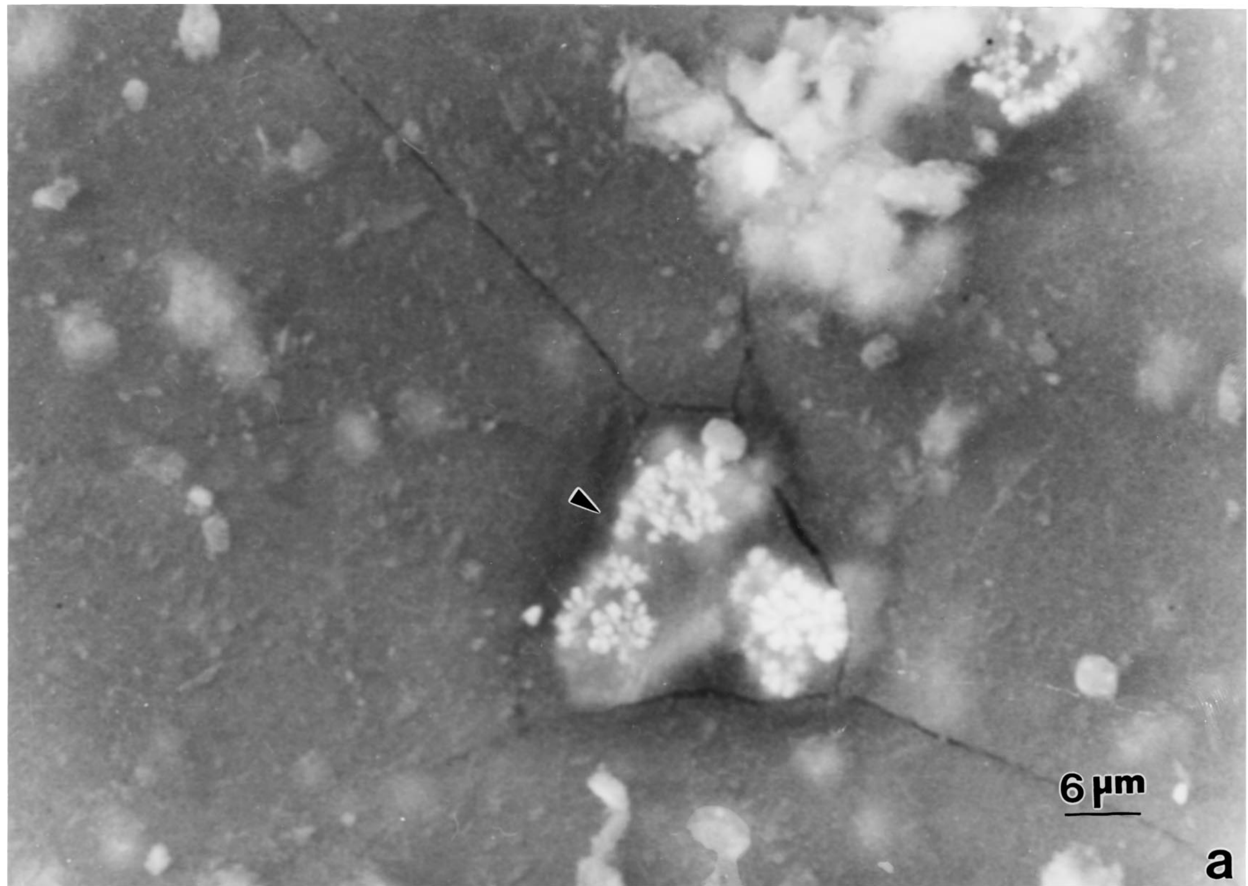

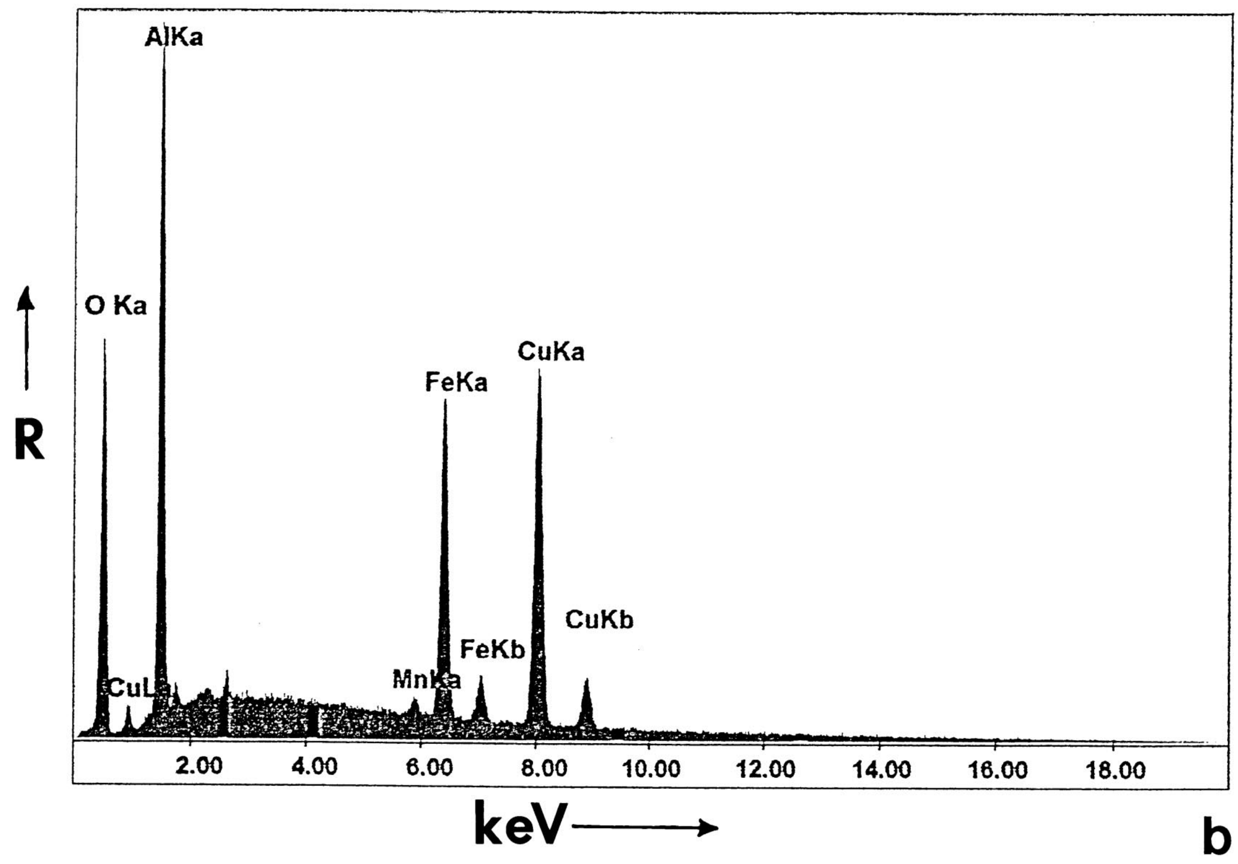

Figure 7 SEM view (a) and EDX spectrum (b) for copper particle clusters (arrow in (a)) observed on aluminum alloy 2024 after exposure to neutral NaCl solution (pH ~ 6).

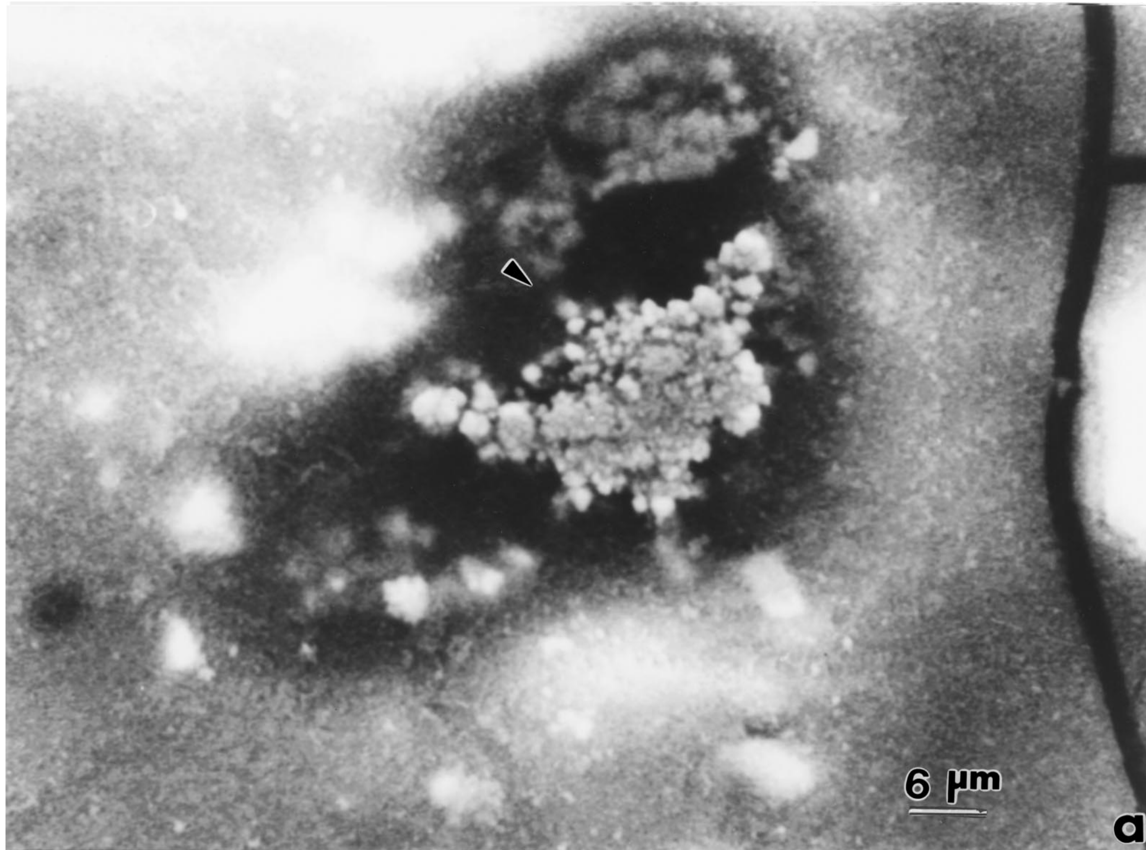

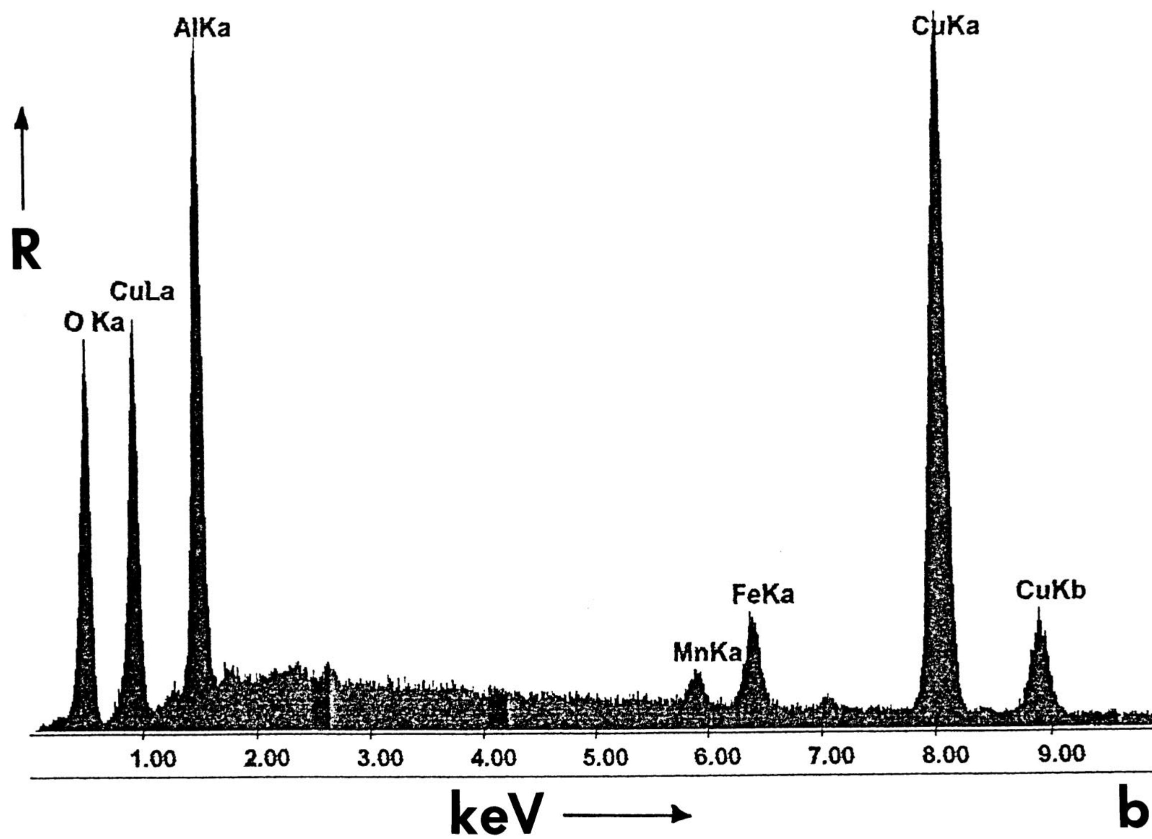

Figure 8 SEM view (a) and EDX spectrum (b) for copper particle cluster on aluminum alloy 2024 at arrow in (a) after exposure to basic (pH 11) NaCl solution.

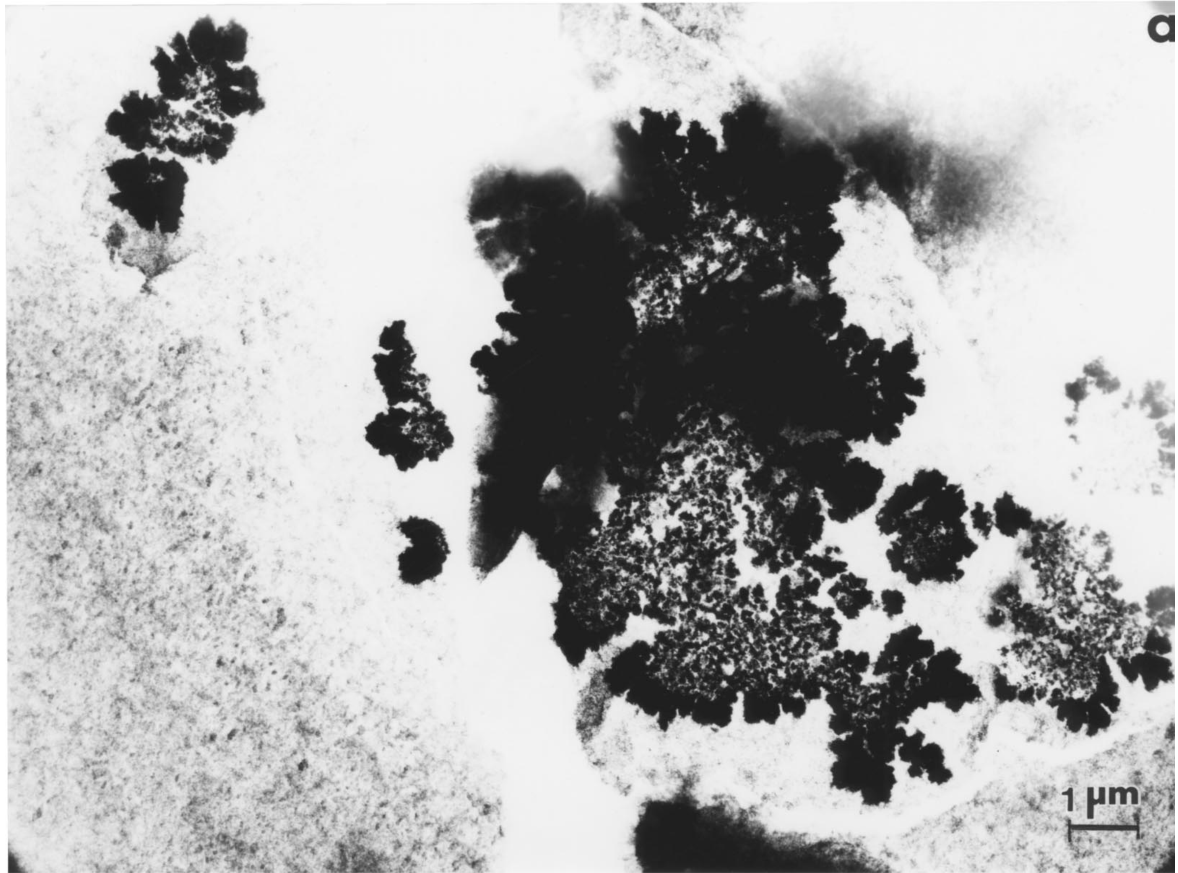

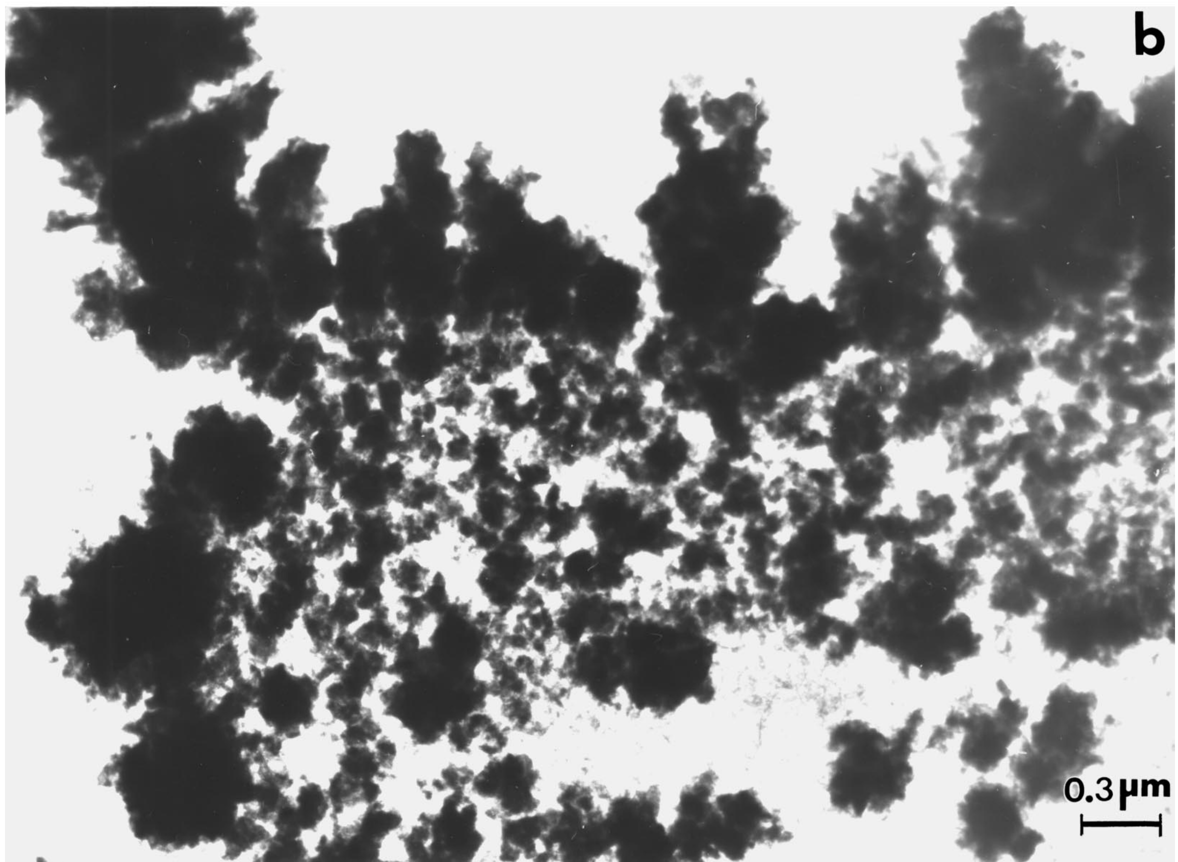

Figure 9 (a) TEM images of copper deposit structure lifted from the surface of aluminum alloy 2024 exposed to neutral (pH 6) NaCl solution. (b) shows a magnified view.

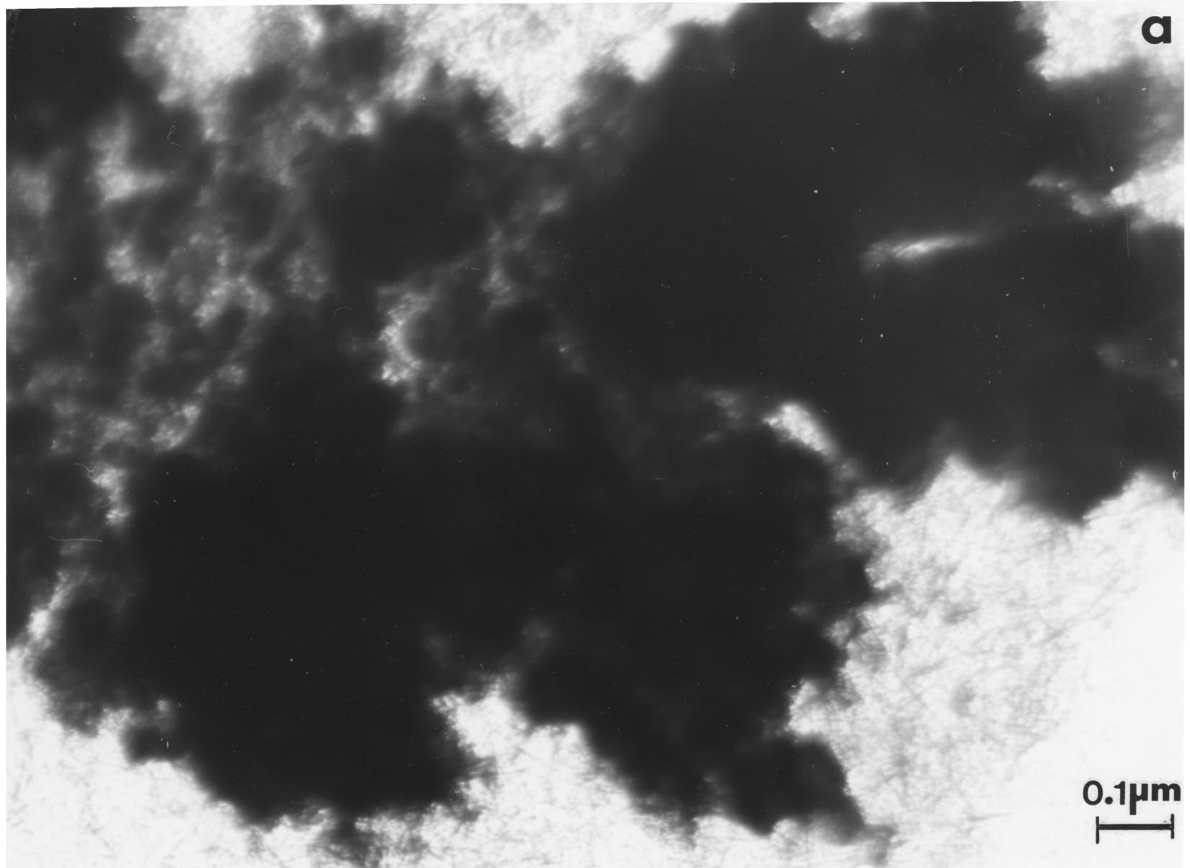

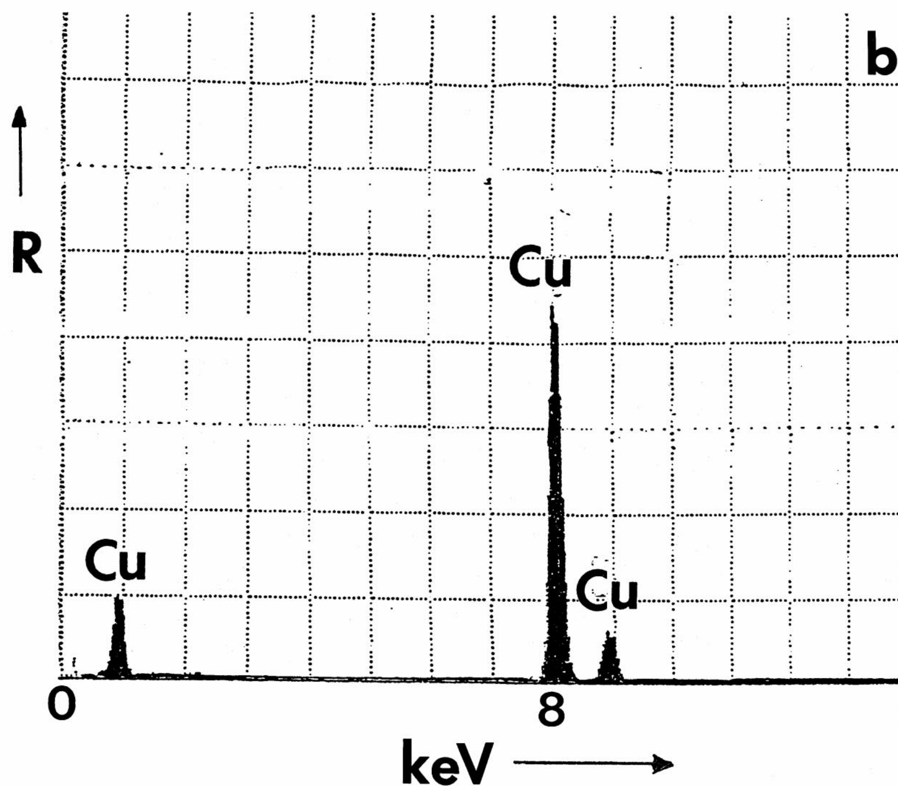

Figure 10 Magnified TEM image of copper deposit on Al 2024 surface exposed in neutral NaCl solution (a) and corresponding EDX spectrum (b).

3.4. Copper nucleation and growth in electrochemical displacement reactions in the Cu/Al cementation system

The copper clusters observed in the SEM views of Figs 7 and 8, and especially the TEM views provided in Figs 9, 11, and 13 look identical to images of copper nucleating and growing on thin aluminum films exposed to $CuSO_4$ solutions for very short times [14]. These solutions, containing 0.5 g/L Cu and 75 mg/L Cl^- ion to remove surface oxides on the aluminum, were also adjusted to a pH of 2.5 with sulfuric acid. These observations of copper nucleation and growth on aluminum

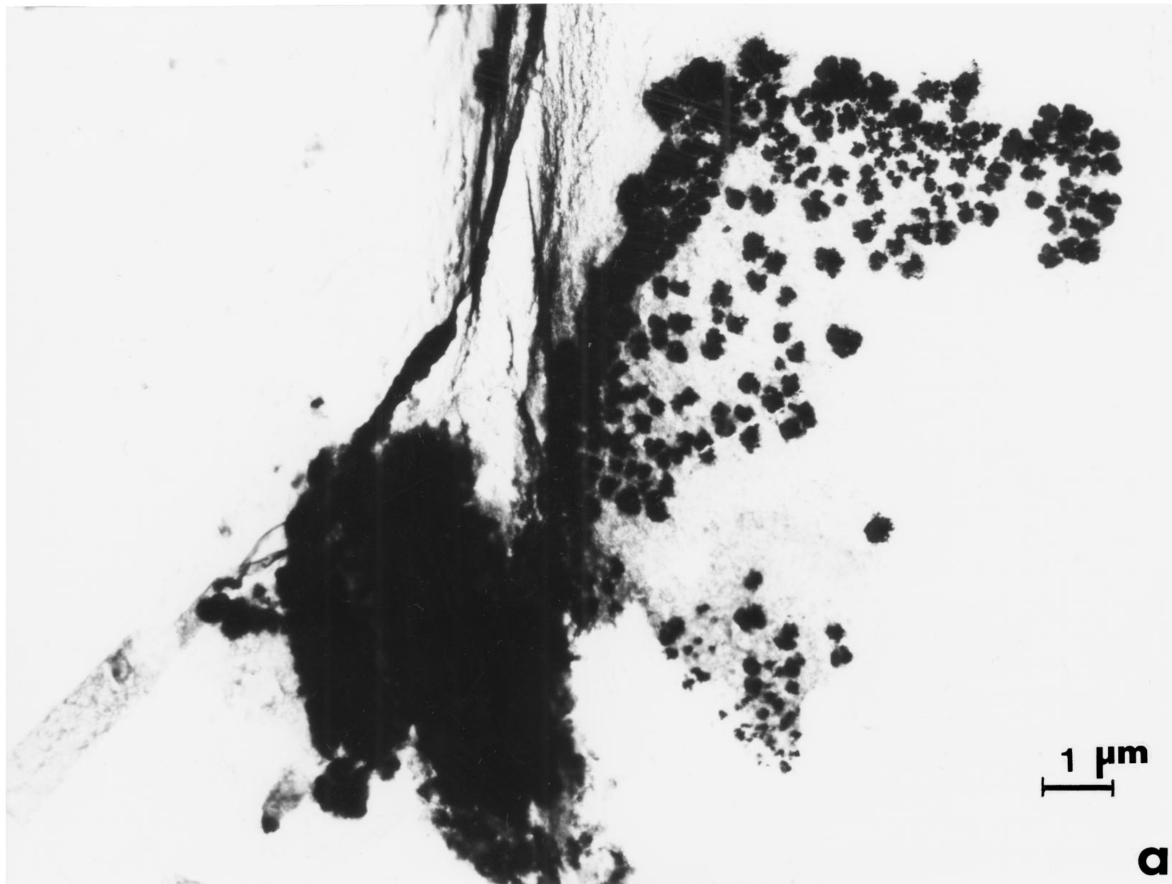

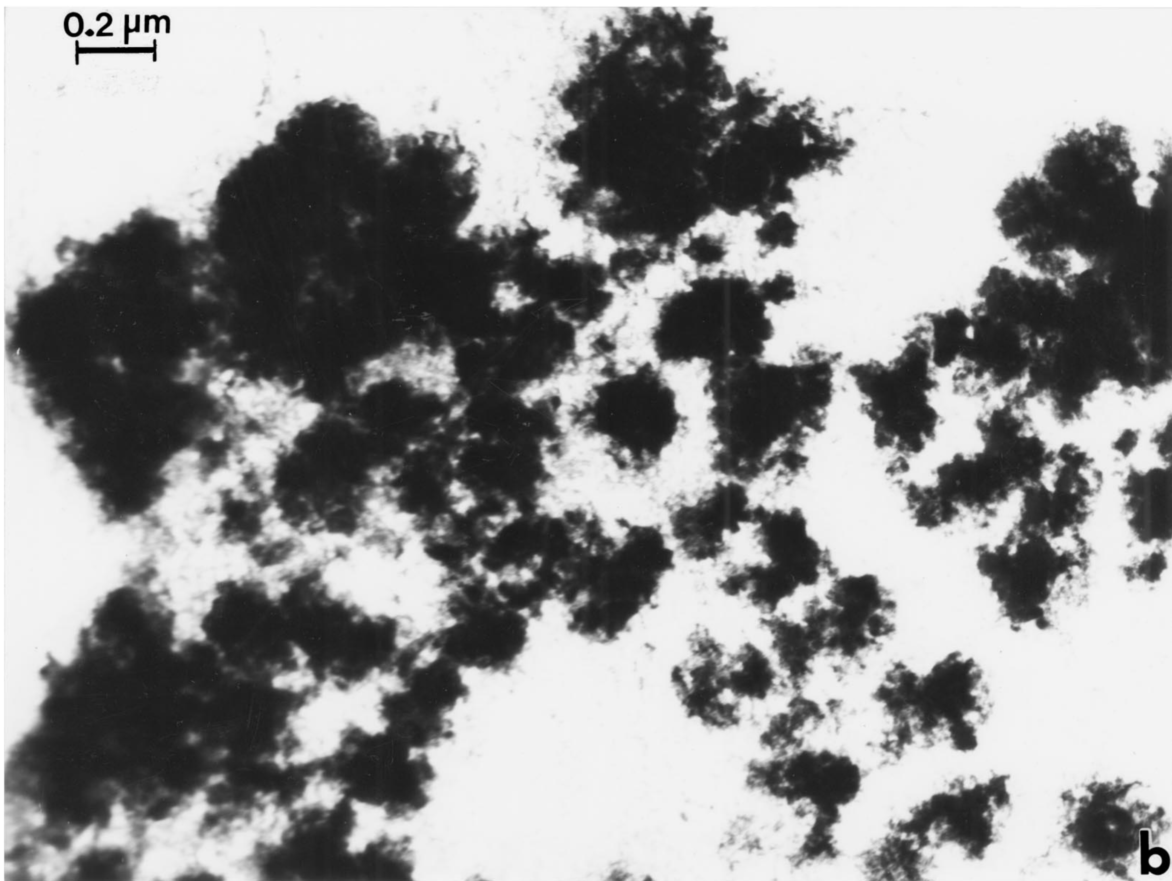

Figure 11 TEM image (a) and magnified view (b) of copper deposit typical for 2024 Al exposed to basic (pH 11) NaCl solution.

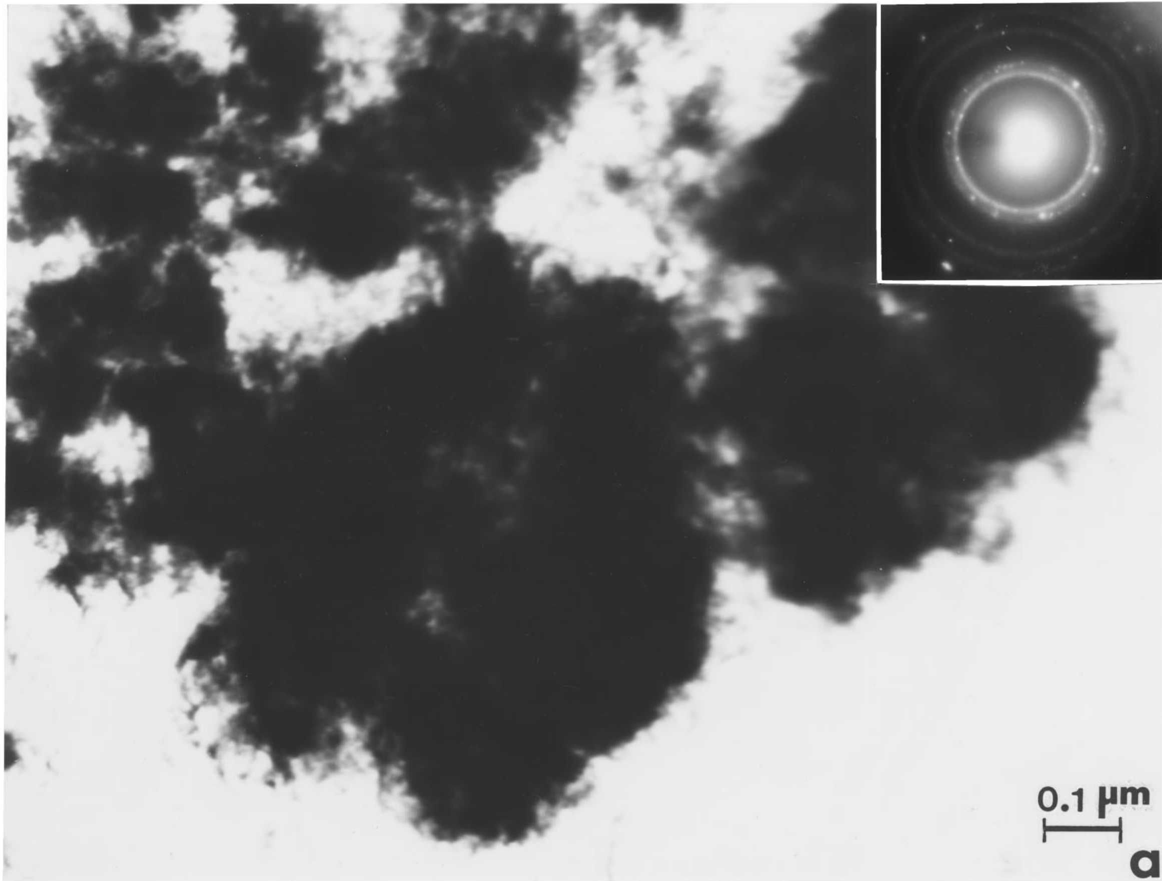

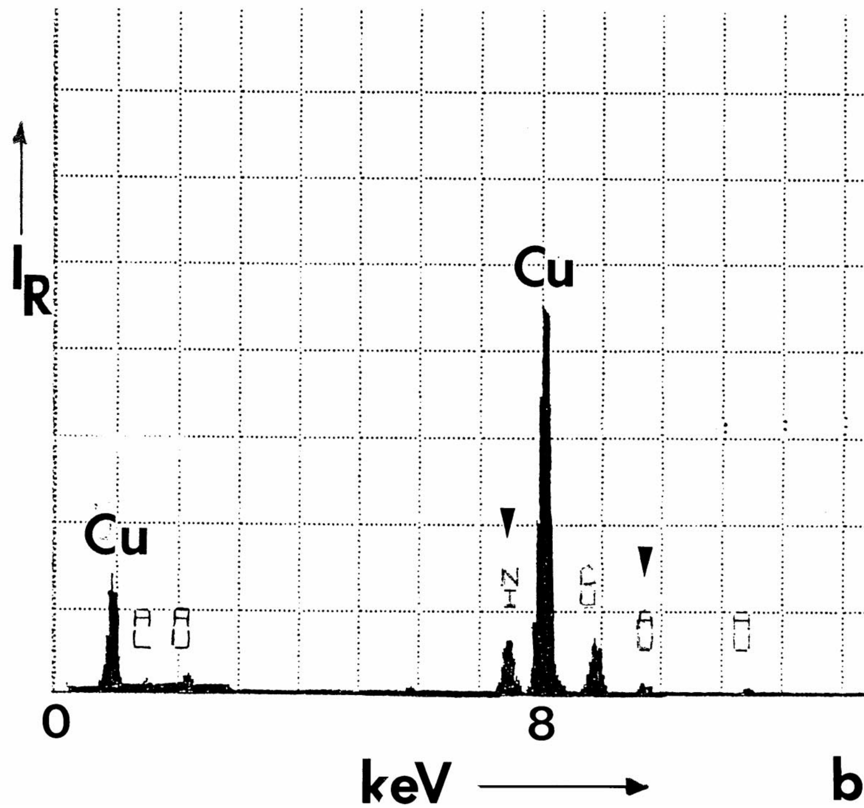

Figure 12 Magnified TEM image of copper deposit on Al 2024 surface exposed in basic (pH 11) NaCl solution (a) and corresponding EDX spectrum (b). Note Ni and Au spectra (arrows) which arise from Ni grid and sputtered Au support film. The selected-area electron diffraction pattern in (a) is copper.

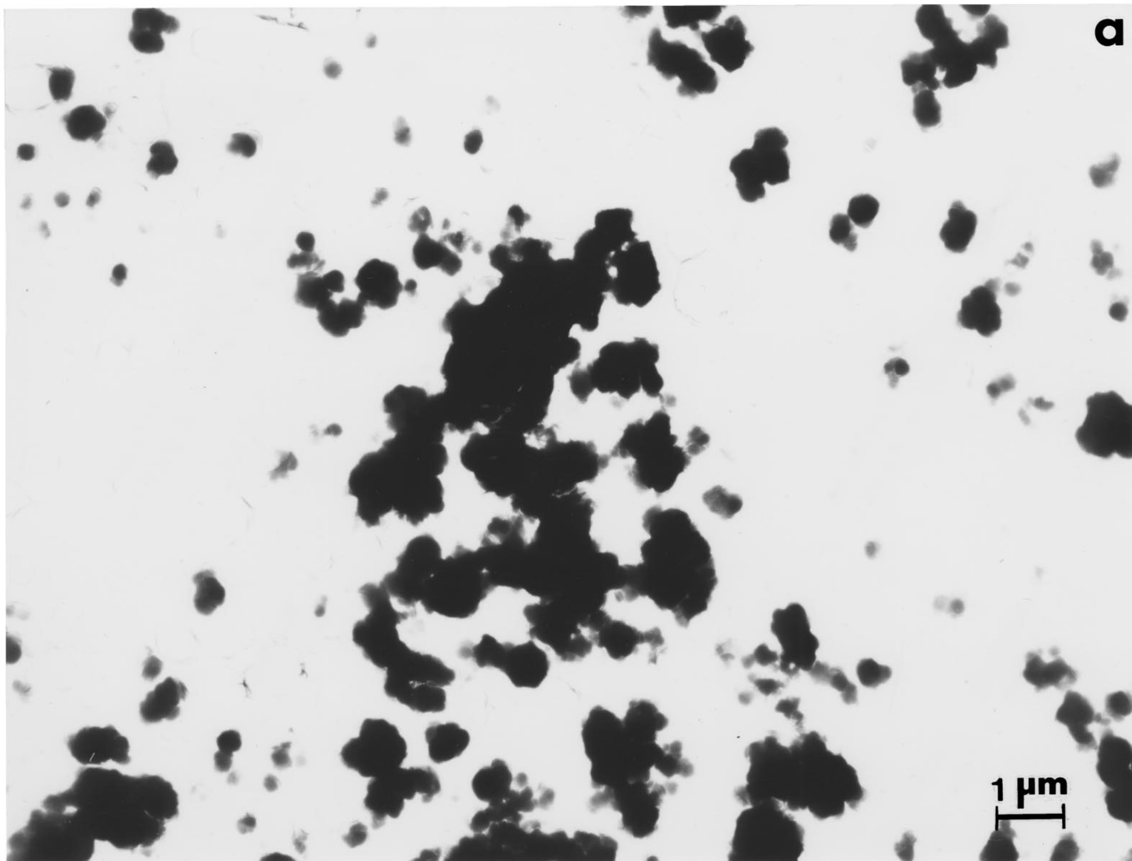

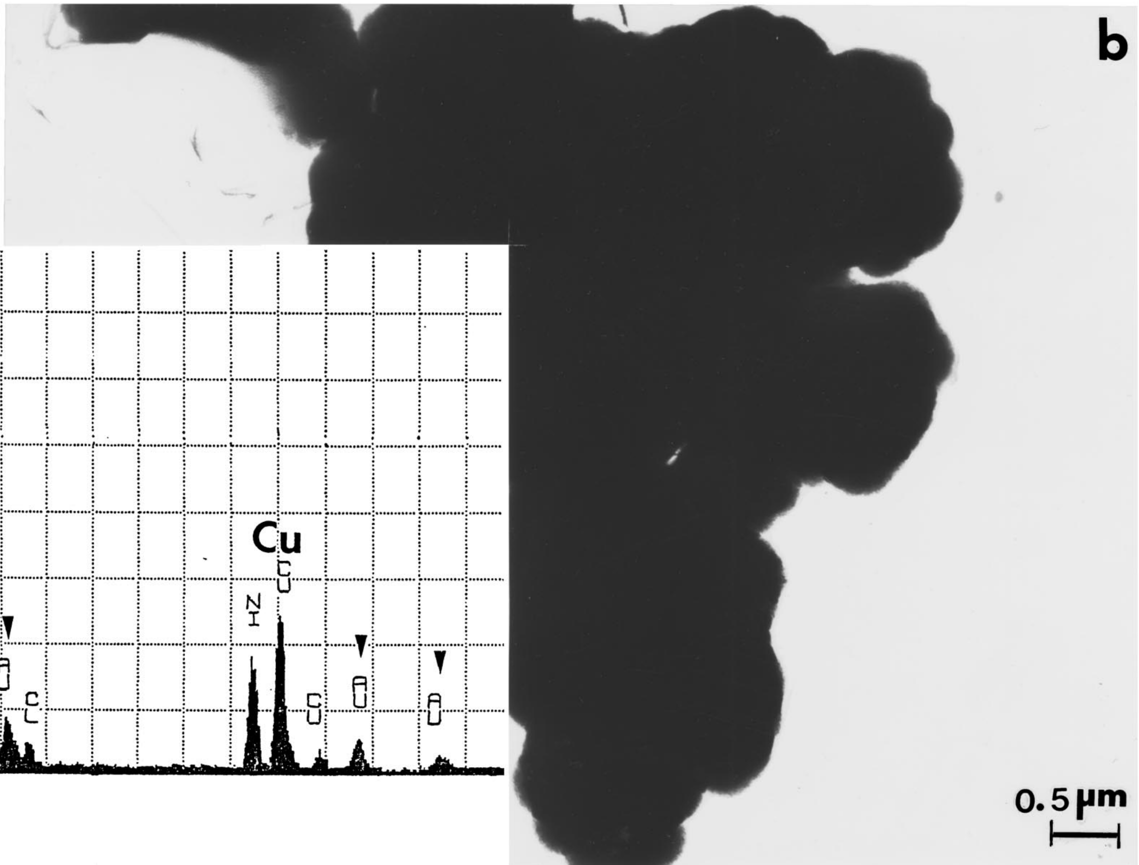

Figure 13 Examples of TEM image features for Cu deposits on Al/2024 coupon surface after exposure to acidic NaCl solution. (a) Lower magnification showing wide distribution of particles and particle clusters. (b) Magnified view of Cu nodule cluster. The EDX spectrum insert shows Ni and the (arrows) spectra from the Ni grid and Au support film. Note presence of Cl peak as well.

surfaces cleaned by Cl^- ion [14], unambiguously confirmed more detailed and extensive kinetic studies of the Cu/Al cementation system by Annamalai, *et al.* [15, 16] which showed that copper deposit structure and morphology was related to kinetics: temperature, pH, concentration, etc. There are also some variations in the copper deposit morphologies shown in Figs 9 and 11 in contrast to Fig. 13 in particular when the pH changes over a range of 11 to 3. Consistent with the earlier work of Annamalai, *et al.* [15, 16], the copper deposits shown in the acidic environment in Fig. 13a is less dendritic and loosely structured and more botryoidal (or nodular), and densely structured than basic or neutral pH environments. Similar results were also obtained by Annamalai, *et al.* [17] for copper plating or deposition onto aluminum alloys (with 1 to 5% Mg additions). In addition, they observed that Cl^- ion was not critical to removing the oxide layer which was much less than that on pure aluminum.

The plating or autodeposition of copper (Cu^{2+}) from solution onto an aluminum matrix is illustrated schematically in Fig. 14. The overall cementation reaction is the combination of the respective half-cell reactions:

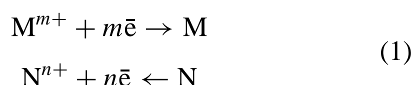

$$\begin{aligned} M^{m+} + m\bar{e} &\rightarrow M \\ N^{n+} + n\bar{e} &\leftarrow N \end{aligned} \tag{1}$$

where $\bar{e}$ is an electron, n and m are integers. With reference to Fig. 14, copper ($M^{m+} = Cu^{2+}$) ions from the NaCl solution are reduced to elemental copper ($M = Cu$) on the more electropositive aluminum (or aluminum alloy 2024) ($N = Al$):

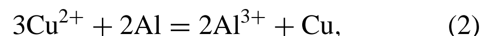

$$3Cu^{2+} + 2Al = 2Al^{3+} + Cu, \tag{2}$$

where $N^{n+} = Al^{3+}$ in Equation 1. For the 2024 Al alloy however, copper is also released back into solution from the substrate corrosion pits (Fig. 14).

In general, aluminum corrosion (pitting) in the presence of Cl^- ion to remove the intrinsic oxide layer and expose anodic metal sites occurs as follows;

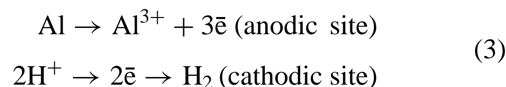

$$\begin{aligned} Al &\rightarrow Al^{3+} + 3\bar{e}\ \text{(anodic site)} \\ 2H^+ &\rightarrow 2\bar{e} \rightarrow H_2\ \text{(cathodic site)} \end{aligned} \tag{3}$$

and when the product (Al^{3+}) $(OH^-)_3$ reaches the saturating product of aluminum hydroxide, the anodic reaction becomes

$$Al + 2OH^- \rightarrow Al(OH)_3 + 3\bar{e} \tag{4}$$

In the presence of dissolved O_2, this reaction can be more complex and result in AlO(OH) products forming. These surface reaction layers may also serve as more electropositive sites for copper deposition because they are semiconducting. In addition, as noted earlier, copper deposition onto Al-Mg alloys was much less sensitive to Cl^- ion [17].

In the recent work of Chen, *et al.* [7], Al-Cu-Mn-Fe-containing particles acted as cathodes during corrosion in slightly acidic NaCl solutions and copper was observed to plate on them (the particles). But copper clusters, appearing similar to those shown in Figs 7–11 were also distributed at other surface sites on 2024 aluminum alloy with no apparent second-phase particle in the vicinity. The morphology of copper deposits also appeared to follow the changes with solution pH as noted in this work.

Since we did not observe any significant Al-Cu-Mg anodic particle activity which may have contributed significantly to the release of elemental copper as noted by Buchheit, *et al.* [5], Dimitrov, *et al.* [6], and even Chen *et al.* [7], the copper in solution must have been released in the anodic aluminum reactions shown in Equation 3 above, in addition to cathodic particles acting as galvanic couples with the aluminum alloy matrix to release Al^{3+} and Cu^{2+}.

To confirm the release of copper ions in solution we measured the copper concentration in the starting (neutral) pH ∼ 6 NaCl solution prior to the start of a corrosion test, using a precision-calibrated atomic absorption spectrometer, to be 0.1 ppm. At the conclusion of a normal test run of 5 days, we remeasured the solution copper concentration; which was observed to have tripled. In a corresponding analysis in both the acidic (pH 3) and basic (pH 11) environments, the ending solution copper concentration doubled. This is an indication that the production of Cu^{2+} in the diffusion boundary layer region illustrated in Fig. 14 probably reached sufficient concentrations to promote copper deposition on surface sites; because the solution was not stirred and

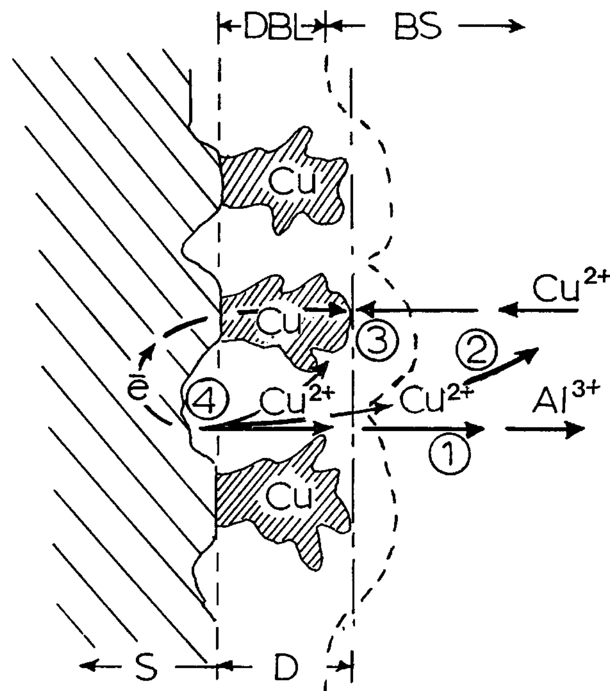

Figure 14 Schematic diagram illustrating copper deposition mechanism. At anodic areas, Al^{3+} and Cu^{2+} ions are released from the alloy into the solution as the alloy corrodes (1 and 2). When the local copper concentration becomes sufficient, copper begins to electrodeposit (3) at favorable (cathodic sites) on the surface. Electrons ($\bar{e}$) are conducted from dissolution sites to the deposition sites (4), allowing the Cu deposit to grow. (After Murr and Annamalai [14].) Figure Key: S - substrate (2024 Al), D - Cu deposit, DBL - diffusion boundary Layer, BS - bulk solution (NaCl).

this process would then appear to be a major contributor to corrosion pitting aluminum alloy 2024 under these circumstances. In this context, the actual concentration of Cu^{2+} in thin aqueous layers on aircraft structures may indeed be high.

3.5. Copper plating/cementation as a corrosion mechanism in 2024 aluminum alloy

It is clear from Fig. 14 that when copper is released into NaCl solutions, especially those having sufficient Cl^- in concentration ($>$75 ppm Cl^-) [14–16] to break down even the most tenacious, intrinsic oxide layers formed on dilute aluminum alloys like 2024, containing sufficient copper additions it can contribute to overall corrosion, and accelerated corrosion, especially pitting corrosion. This is true especially in relatively static environments where a high concentration of Cu^{2+} can accumulate next to the exposed alloy matrix surface. Variations in the pH, as noted in this work, can alter the integrity and morphology of copper deposits which in turn can affect the efficiency of pitting corrosion. That is, the nodular Cu deposits formed in acidic NaCl environments may be more adherent than those in neutral or basic environments, thereby influencing the frequency of corrosion pits in the matrix (Fig. 14). However temperature will have an important influence as well [15–17]. In fact, copper deposition as a contributor to pitting corrosion may be as common as variations in the propensity of second-phase particles which act, variously, as anodic and cathodic sites relative to the aluminum alloy matrix. Certainly the role played by constituent (second-phase) particles in aluminum alloys is an important issue in pitting corrosion, but the complex, galvanic cells which can characterize the exposed aluminum (alloy) surface in aqueous environments can include the coupling of various particle compositions with copper deposition sites. Copper deposition onto iron-rich precipitates as noted in this work and in other studies [7] may also involve a reaction of the form

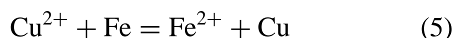

$$Cu^{2+} + Fe = Fe^{2+} + Cu \quad (5)$$

where the iron-containing precipitate becomes the more electropositive substrate. However, the standard free energy change associated with the precipitation or plating of copper onto iron as shown in Equation 5 is -36 kcal/mol at 25°C in contrast to -92 kcal/mol for copper onto aluminum as shown in Equation 2 [18]. It should of course be noted that in many corrosion situations, as opposed to copper concentration from relatively concentrated solutions, other cathodic processes may also make significant contributions in addition to Cu deposition. Consequently there may not be a one-to-one ratio of Cu atoms deposited to Al^{3+} ions released to solution.

4. Summary and conclusions

Commercial, aging aircraft/airframe 2024 aluminum alloy was observed to contain clusters of copper and copper-rich particles at inclusions and at other surface sites following free corrosion immersion experiments for 5 days in basic (pH 11), neutral (pH $\sim$ 6) and acidic (pH 3) sodium chloride solutions (0.6 M NaCl). TEM analysis conducted to perform an inventory of second-phase particles in this alloy showed essentially 5 prominent regimes of particles and particle clusters: Al-Fe-Cu-Mn, Al-Cu-Si, Al-Cu-Mg Al-Cu-Fe-Mn-Si, and Al-Cu-Fe. The Al-Cu-Mg-containing particles were not as common as other 2024 Al alloys, and there was often a propensity of iron-containing particles associated with clusters of copper, indicative of the plating out of copper in solution onto these cathodic particles.

A slightly modified replication technique was used to lift particles and other products from the surface of the 2024 aluminum alloy coupons following immersion in the NaCl solutions. These lift-off samples were examined in the TEM and extensive deposits and clusters of copper were observed not only at apparent precipitate sites, but at other, random sites. These copper deposits consisted of very fine, microdendritic growths in basic and neutral NaCl solutions but became botryoidal or nodular in acidic NaCl solutions. These observations are consistent with electrochemical displacement reactions where copper in Cl^- solutions is deposited onto a more electropositive aluminum substrate. In this reaction on aluminum alloy 2024, Cu^{2+} concentrates in a solution layer at the metal surface and nucleates and grows, causing additional pitting corrosion; releasing Al^{3+} and some Cu^{2+}. Consequently, in NaCl environments where the Cl^- ion removes any surface oxide, copper-containing aluminum alloys will exhibit enhanced pitting corrosion as a consequence of copper deposition (cementation) on the aluminum alloy surface, and possibly on more electropositive inclusions exposed at the surface.

Acknowledgements

This research was supported by the Air Force Office of Scientific Research (F49620-95-1-0518) through the FAST Center for Structural Integrity of Aerospace Systems at The University of Texas at El paso. We are grateful for the help of Dr. Walter Fisher in clarifying electrochemical issues and to C. J. Miglionico of the Air Force Phillips Laboratory, Kirkland AFB, New Mexico for helping in the development of the lift-off technique.

References

1. "Air Force Blue Ribbon Advisory Panel on Aircraft Coatings, Part 1: Basic Research" (Wright Laboratory, Aeronautical Systems Center, Air Force Systems Command, 1995). Prepared for Materials Directorate, Wright-Patterson AFB, Ohio.
2. R. G. BUCHHEIT, *J. Electrochem. Soc* **142** (1995) 3994.
3. A. GARNER and D. TROMANS, *Corrosion* **35** (1979) 55.
4. K. URISHINO and K. SUGIMOTO, *Corrosion Sci.* **19** (1979) 225.
5. R. G. BUCHHEIT, R. P. GRANT, P. F. HLAVA, B. MCKENZIE and G. L. ZENDER, *J. Electrochem. Soc.* **144**(8) (1997) 2621.
6. N. DIMITROV, J. A. MANN and K. SIERADZKI, *ibid.* **146**(1) (1999) 98.
7. G. S. CHEN, M. GAO and R. P. WEI, *Corrosion Science* **52**(1) (1996) 8.

8. R. P. WEI, C-M. LIAO and M. GAO, *Metall. and Mater. Trans. A* **29A** (1998) 1153.
9. C. MIGLIONICO, C. STEIN and L. E. MURR, *J. Mater. Sci.* **26** (1991) 5134.
10. L. E. MURR and W. H. KINARD, *American Scientist* **81**(March–April) (1993) 152.
11. A. MUNITZ, A. ZANGVIC and M. METZGER, *Met. Trans. A* **11A** (1980) 1863.
12. M. GAO, C. R. FENG and R. P. WEI, *Metall. and Mater. Trans. A* **29A** (1998) 1145.
13. ASM HANDBOOK, Vol. 13: Corrosion (ASM International Materials Park, OH, 1987) p. 584.
14. L. E. MURR and V. ANNAMALAI, *Metall. Trans. B* **9B** (1978) 515.
15. V. ANNAMALAI, J. BRENT HISKEY and L. E. MURR, *Hydrometallurgy* **3** (1978) 163.
16. V. ANNAMALAI and L. E. MURR, *ibid.* **3** (1978) 249.
17. V. ANNAMALAI, J. B. HISKEY and L. E. MURR, *Trans. Soc. Mining Engrs. of AIME* **266** (1979) 1963.
18. L. E. MURR, *Mineral Sci. Engng.* **12**(3) (1980) 121.

Received 2 August 1999
and accepted 10 February 2000